Journal homepage: http://gwse.iheg.org.cn

Research Paper

Exploring the groundwater response to rainfall in a translational landslide using the master recession curve method and cross-correlation function

Cheng-peng Ling[1], Qiang Zhang[1,2*]

[1] *Chengdu University of Technology*, *Chengdu* 610059, *China*.
[2] *State Key Laboratory of Geohazard Prevention and Geoenvironment Protection (Chengdu University of Technology)*, *Chengdu* 610059, *China*.

Abstract: Rainfall is a common trigger for landslide reactivation, as it raises groundwater levels and reduces bedrock or soil shear resistance. This study focuses on the Kualiangzi landslide in the southern region of Sichuan Province, China. Real-time monitoring of groundwater levels and rainfall from July 2013 to September 2016 is analyzed. Groundwater table increments, considering groundwater drainage rate, were calculated using the water-table fluctuation and master recession curve method and the response time of the groundwater table to rainfall events was estimated using the cross-correlation function. Results reveal that groundwater level declines from tension troughs to landslide fronts in the rainy season, with a significant positive correlation between the groundwater level in the tension trough and landslide surface displacement. Evaluated spring elevations for groundwater discharge range from 410 m to 440 m, which is in agreement with the actual spring elevations (390–423 m). Lag times of groundwater response to rainfall decreases with cumulative rainfall of the rainy periods. In the middle part of the landslide, two responses between rainfall and groundwater levels indicate two water movement pathways: Vertical cracks or fractures resulting from the slow landslide movement, and matrix pore space in unconsolidated sediment. Variations in peak values of the cross-correlation function suggest early dominance of the uniform matrix flow and later dominance of preferential flow during the rainy period.

Keywords: Translational landslide; Rainfall; Groundwater; Lag response; Water table fluctuation; Recharge pathway

Received: 22 Nov 2023/ Accepted: 26 Apr 2024/ Published: 10 Aug 2024

Introduction

Traditional landslides are common in the Sichuan Basin of Southwest China, characterized by nearly horizontal bedrock composed of sandstone and mudstone with a dip angle commonly less than 10° (Fan et al. 2009). These landslide, known for their complex mechanisms and severe damage, are caused by the differential behavior of sandstone and mudstone, leading to the gradual development of vertical cracks or fractures in the slope. These fractures increase groundwater recharge and stratum hydraulic conductivity. During the rainy season, intense rainfall can infiltrate these fractures, raising groundwater pressure and reducing the effective shearing resistance of mudstone acting as the sliding surface (Fan et al. 2009; Zhang et al. 2015; Leng et al. 2022). Understanding the impact of rainfall events on groundwater fluctuations and slope stability is crucial for analyzing sliding mechanisms and preventing hazards.

The process of water infiltration into landslide after precipitation, leading to eventual movement, is complex and influenced by various factors such as topography, geology, and meteorology (Wen et

*Corresponding author: Qiang Zhang, *E-mail address*: lingcp2015@163.com

DOI: 10.26599/JGSE.2024.9280018

Ling CP, Zhang Q. 2024. Exploring the groundwater response to rainfall in a translational landslide using the master recession curve method and cross-correlation function. Journal of Groundwater Science and Engineering, 12(3): 237-252.

al. 2004). Analyzing the relationship between precipitation and landslide occurrence often involves statistical techniques like the impulse response model and the output-error model. These methods help determine critical thresholds for daily and antecedent rainfall that trigger sliding (Bernardie et al. 2015; Vallet et al. 2016; Shah et al. 2023). Additionally, studies have assessed the impact of groundwater on landslide stability. The limit-equilibrium methodology, which considers pore water pressure, remains a widely applied approach for evaluating slope stability (Glade and Crozier, 2005; Xu et al. 2016; Song et al. 2021).

Besides researching the influences of the groundwater level on slope stability, the understanding the response of groundwater levels to rainfall is crucial for geohazard prevention. The time delay between rainfall and slope sliding is valuable for early warning systems to protect residents and property. Research by Luna and Korup (2022) revealed a seasonal pattern of landslide activity in the Pacific Northwest, with the highest probability occurring in January, lagging behind the annual peak precipitation. Similarly, Hou et al. (2022) investigated the failure characteristics and mechanisms of a landslide that occurred 42 hours after previous rainfall in Zhonghai Village, Hanyuan Country, China.

The relationship between groundwater levels and precipitation has drawn significant attention from hydrologists and hydrogeologists (Jan et al. 2007; Hong and Wan, 2011). Over the past two decades, there have been considerable advancements in automatic monitoring technologies in hydrogeology. The increase in both the quantity and quality of monitored data has facilitated the utilization of time series models with data-based learning algorithms to predict groundwater level fluctuations in response to rainfall (Sahoo and Jha, 2013; Ciupak et al. 2015; Yan and Ma, 2016; Yoon et al. 2016).

The fluctuation of groundwater table is considered the most fundamental and critical information in hydrogeology. Healy and Cook (2002) provided a comprehensive review of the Water-table Fluctuation (WTF) methods, highlighting their simplicity and insensitivity to the mechanisms governing water movement through the vadose zone. Nimmo et al. (2015) introduced a discrete-storm WTF method to estimate episodic recharge, while Crosbie et al. (2019) proposed an approach to constrain the magnitude and uncertainty of specific yield in the WTF method for groundwater recharge estimation. Maréchal et al. (2023) analyzed the influence of the location of observation wells on groundwater recharge estimation in various regions, including Eastern Canada and Thailand (Labrecque et al. 2020; Tesfaldet et al. 2020).

The relationship between rainfall and groundwater table dynamics in translational landslides is often intricate due to the varying characteristics of rainfall events and the moisture content of the unsaturated zone. This paper presents the findings of a comprehensive monitoring study conducted on the groundwater table and precipitation from June 2013 to September 2016 in the southern area of the Kualiangzi landslide, a representative translational landslide located in Southwest China. The study employs the Water-table Fluctuation (WTF) method and master recession curve analysis to compute the corrected increments of the groundwater table influenced by rainfall. Additionally, the effects of rainfall events with different characteristics on the water table and the lag time between them are analyzed through cross-correlation analyses. These findings contribute to the development of models simulating the groundwater table response to the rainfall, which can, in turn, aid in predicting slope stability and landslide displacement under certain rainfall conditions. Such models hold significant potential for enhancing early warning systems aimed at mitigating landslide hazards.

1 Geographyical, geological, geotectonic, and hydrological settings

The Kualiangzi landslide is located approximately 65 km southwest of Zhongjiang County in the Sichuan province, China (Fig. 1a and 1b). It occupies a geomorphic unit characterized by tectonic erosion, resulting in a valley with a width ranging from 50 m to 300 m and a depth of 100 m to 170 m. Positioned within the northern flank of the Cangshan anticline, the landslide is situated in an area where the bedrock generally dips to NW20-30° at an angle of 2–5° (Fig. 1b). Notably, there are no faults or historical records of destructive earthquakes in the study area.

The main body of the landslide spans approximately 1,100 m in width and measures between 360 m and 390 m in length (Fig. 1c). It boasts an averages thickness of around 50 m, with its maximum thickness reaching 80 m (Fig. 1d). The rear edge of the landslide forms the main scarp, extending in a N-S direction. At the toe front edge, an uplift belt is visible, along with several toe slips and seasonal springs. The elevation disparity between the toe front and the main scarp is approx-

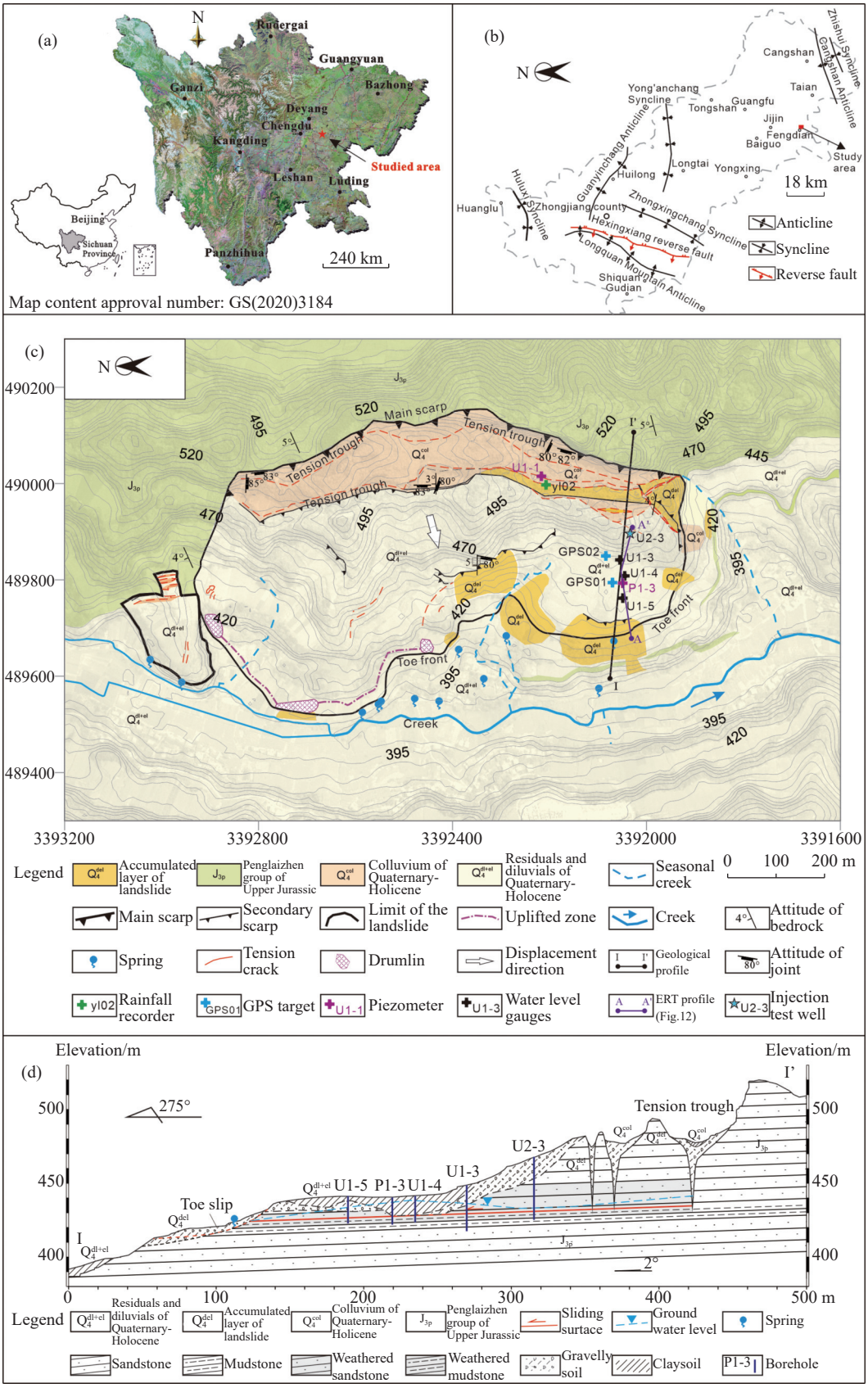

Fig. 1 Study area

(a) Location of the study area in Sichuan Province. (b) Tectonic outline map in the Zhongjiang District. (c) Geological schematic map of the Kualiangzi landslide. (d) Geological profile of section I-I' (modified from Ling et al. 2016). The geographic data set is provided by Geospatial Data Cloud site, Computer Network Information Center, Chinese Academy of Sciences http://www.gscloud.cn).

imately 110 m. Overall, the area covered by the Kualiangzi landslide spans 0.51 km^2, with a volume estimated at 25.5 million m^3 (Zhai, 2011; Xu et al. 2016).

The area where the landslide is situated falls within the subtropical and monsoonal climate zone. According to the rainfall data collected from the landslide site, the average annual precipitation is 844.5 mm, with more than 80% of the total precipitation occurs during the rainy season from June to September (Xu et al. 2016). Rainfall during this period is characterized by high frequency, prolonged duration, and substantial cumulative precipitation.

The Kualiangzi landslide has exhibited a consistent pattern of slow westward creeping over time, although this displacement can accelerate during periods of intense rainfall, particularly in the rainy season. Initially, a series of aligned soil holes, each deeper than 50 m, were observed on the surface along the rear edge of the landslide. These holes gradually connected through the formation of a large and elongated crack. During the rainy season of 1949, the first rapid acceleration in displacement occurred due to heavy rainfall, leading to the creation of a large-scale tension trough extending in a N-S direction (Fig. 1c). The second significant acceleration in displacement was triggered by intense rainfall during the rainy period of 1981, resulting in widespread destruction of houses and the forced migration of residents. In subsequent decades, the tension trough near the main scarp significantly widened, reaching a width of 60 m and a length of 1 km. In addition to these large-scale tension troughs, two sets of subvertical joints formed in the NW10-20° and SW10-29° directions, with dipping angles ranging from 80° to 85° and 72° to 82°, respectively. Numerous minor tension fractures were also induced by the gradual creeping of the landslide.

The bedrock underlying the landslide consists of sandstone interbedded with mudstone and siltstone, forming part of the Penglaizhen group, which was deposited during the Upper Jurassic period (J_3p). The sandstone typically has a thickness ranging form several meters to tens of meters and dips at an angle of approximately NW20-30° with a gentle inclination of 2°–5°. In contrast, the mudstone, characterized by good water-absorbing structures and low strength, predominates in the sliding zone (Fan et al. 2009; Xu et al. 2016). According to the drilling core samples, the mudstone layer varies in thickness from 0.5 m to 2 m along the main sliding surface. On the surface of the landslide, a layer of residuals and diluvials (Q_4^{el+dl}) is predominantly present, with a thickness ranging from 1 m to 13 m. Comprising silty clay mixed with gravels, these residuals and diluvials contribute to the surficial composition. Within the tension trough, unconsolidated sediment known as colluvium (Q_4^{col}) is prevalent, composed of rock blocks, gravels, and breccias. Notably, the rock blocks within the colluvium can attain a maximum diameter of 5 m. The thickness of colluvium ranges from 51 m to 72.9 m (Zhai, 2011).

The dense cracks or fractures resulting from the creeping of the landslide serve as crucial conduits for storing the groundwater, forming the primary unconfined aquifer within the landslide. This groundwater reservoir is primarily replenished by precipitation. The groundwater level within the tension trough assumes a pivotal role in controlling the displacement behavior of the landslide (Fig. 1d). Field monitoring data reveals a close correlation between the rise in groundwater level within the tension trough and the displacement rate of the landslide. The positive pore water pressure exerted on the rear edge of the landslide serves as the driving force behind its movement, as evidenced by previous studies (Fan et al. 2009; Xu et al. 2016; Ling et al. 2016).

Lv et al. (2019) conducted two tracer tests and one injection test at the U2-3 borehole (Fig. 1c and 1d). The hydrological tests revealed the presence of two distinct groundwater runoff modes within the landslide: the concentrated mode and the dispersed mode. In the concentrated mode, groundwater primarily flows through subvertical cracks oriented in the NW10-20° direction within the sandstone layer. These subvertical cracks, induced by the creeping of landslide, are nearly perpendicular to the direction of sliding. Conversely, in the dispersed mode, groundwater follows the bedding planes of both sandstone and mudstone, exhibiting significantly lower flow velocities compared to the preferential flow pathways. Multi-tracer test results indicated that the hydraulic conductivity perpendicular to the sliding direction was approximately 813.6 m/d, whereas along the sliding direction, it was approximately 0.216 m/d (Lv et al. 2019).

2 Investigation methods

2.1 Core drilling

Comprehensive engineering geological exploration has been carried out in the landslide area since 2010. Twenty-three boreholes were drilled in the southern area of the landslide in 2010, 2013, and

2014 (Ling et al. 2016). The lithology, stratum thickness, core recovery parameters, and static groundwater level in each borehole were recorded. In this study, several boreholes (i.e. U1-1, U1-3, U1-4, U1-5, and P1-3) were specifically selected for groundwater level monitoring purposes (Fig. 2).

2.2 Field real-time monitoring

In the southern area of the landslide (Fig. 1c), several monitoring instruments were installed. Two Global Navigation Satellite System (GNSS) receivers (BDStar Navigation) were used to monitor the surface displacement with an accuracy of 10^{-5} mm, operating at a frequency of once per hour. A tilting rain gauge (Tianjin Smart Sensor Technology Co., Ltd) was installed at yl02 to monitor rainfall with an accuracy of 0.2 mm, and the monitoring frequency is twice per hour. Vibrating wire piezometers (BGK4500, Geokon) were installed at U1-1 and P1-3 to monitor pore-water pressure with an accuracy of 1 Pa. Radar sensors (BGK 3950,

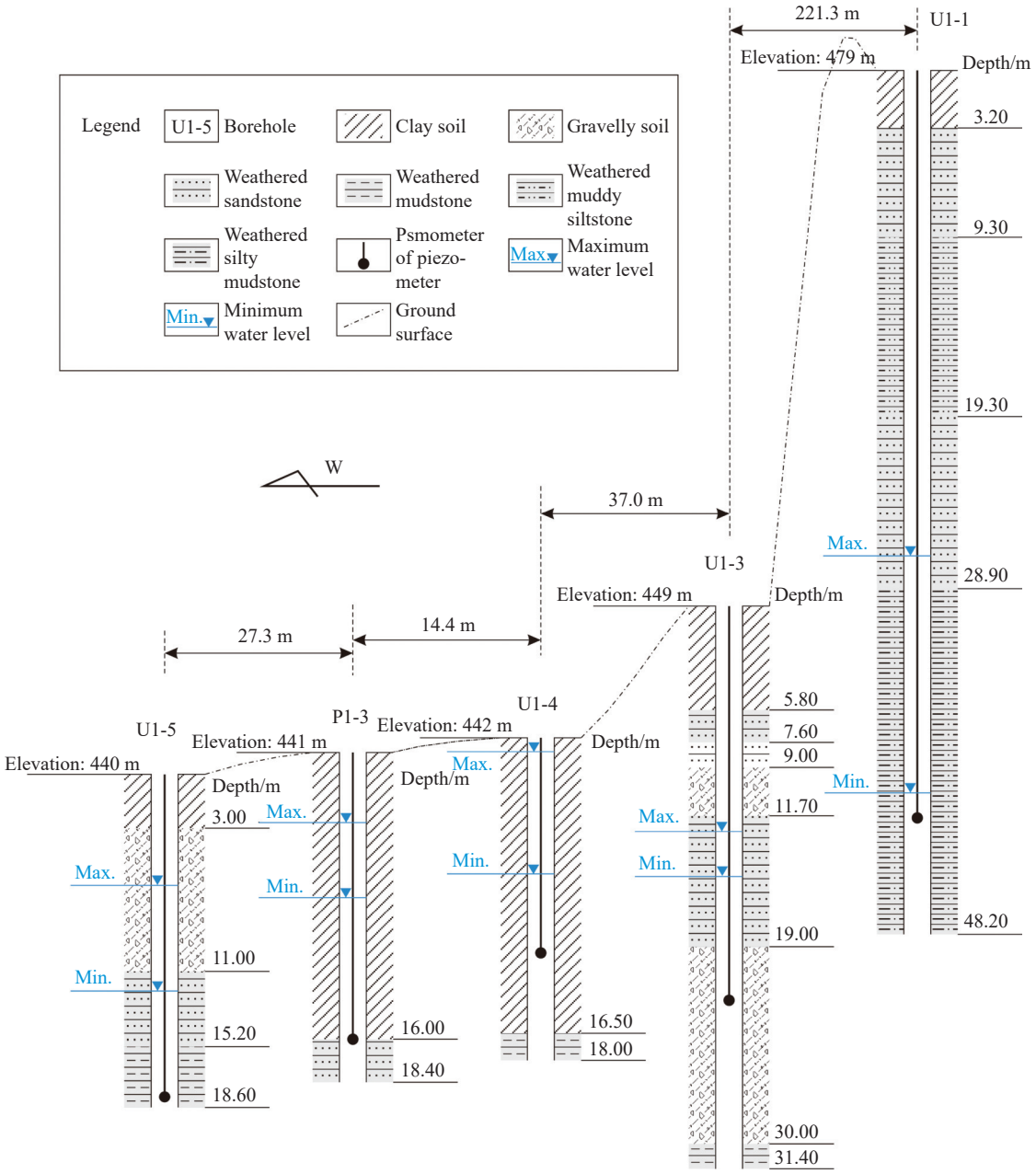

Fig. 2 Lithology, stratum thickness, and water level sensors in the boreholes U1-1, U1-3, U1-4, U1-5, and P1-3. The maximum and minimum of the water table in each borehole were obtained from 1 June 2013 to 12 September 2016

Note: the length and surface elevation of each borehole were drawn on a same vertical scale, but not a same horizontal scale.

Geokon) were installed at U1-3, U1-4, and U1-5 to monitor groundwater level with an accuracy of 1 mm.

Several vibrating wire piezometers and radar sensors were damaged due to the creeping of the landslide. Data from piezometers U1-1 and P1-3, as well as water level gauges U1-3, U1-4, and U1-5 (Fig. 1c) from 1 June 2013 to 12 September 2016 were used to analyze the groundwater level response to rainfall. The hourly values of piezometric water level or pressure were automatically measured for P1-3, U1-3, U1-4, and U1-5. For U1-1, groundwater pressure was measured every six hours from 1 June 2013 to 7 August 2013, and once an hour thereafter. The groundwater level was calculated from the osmotic pressures of U1-1 and P1-3. Abnormal hourly data were first removed to prevent artifacts.

2.3 The corrected increment of the groundwater table by rainfall

Throughout this paper, groundwater tables are reported in terms of total head (H for the daily value, and h for the hourly value) above sea level. To calculate the increment of groundwater table by rainfall, a rainfall event is defined as a continuous period of recorded rainfall, separated from other events by at least a 48-hour interval with a rainfall amount of less than 2 mm. During the monitoring activities, a total of 86 rainfall events were recorded.

The groundwater table is a parameter characterizing the interaction between groundwater recharge and discharge. When recharge exceeds discharge, the groundwater table rises, and vice versa. However, there's an important consideration related to rainfall-induced changes. When the measured groundwater level increases due to rainfall, the drainage rate of groundwater also increases with the increment of the groundwater level. Hence, the calculated groundwater table increment, obtained by subtracting the measured water table of the previous time step from the water table of the present time step during rainfall, may underestimates the true value (Fig. 3a). Considering the drainage rate of groundwater, the corrected daily increment of the groundwater table due to a rainfall event can be calculated using the following equation, derived from the WTF method employed by Crosbie et al. 2005).

$$H_t^{Inc} = (H_t - H_{t-1}) + D(H_{t-1}) \cdot \Delta t \quad (1)$$

Where: H_t^{Inc} is the daily increment of the groundwater table at time t (day); H_t and H_{t-1} are

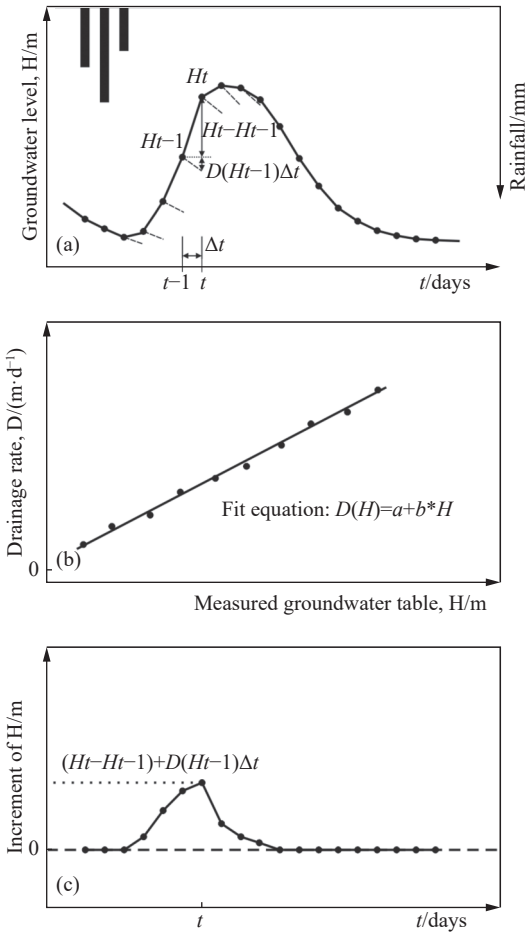

Fig. 3 Schematic diagram for calculating the groundwater table increment by a rainfall event

(a) The measured water level process line after a rainfall event. (b) The relationship between measured water level (H) and drainage rate (D>0) if the groundwater level varies with a large range. (c) The corrected groundwater table increment considering the drainage rate of the groundwater.

groundwater tables at time t and $t-1$, respectively. Δt is the time step. The increment of groundwater table is only calculated on days where the rainfall occurs, i.e. $(H_t - H_{t-1}) + D(H_{t-1}) \cdot \Delta t > 0$ and $\sum_{t>t'>t-\alpha} P_{t'} > 0$. P_t is the daily rainfall at time t (day). The values of α are the maximum lag time before the water level rises according to the 86 rainfall events. $D(H_{t-1})$ is the drainage rate (>0, m/d) at the groundwater table H_{t-1}, which accounts for how far the water table would have fallen. The drainage rate $D(H)$ can be obtained from the decreasing groundwater level (H) in the period without a rainfall event.

Fig. 4 depicts the diagram of groundwater discharge in the landslide. The hydraulic conductivity of the aquifer is denoted by K. The groundwater level at the borehole in Fig. 4 is H at time t_1. The cross-sectional area for groundwater runoff is

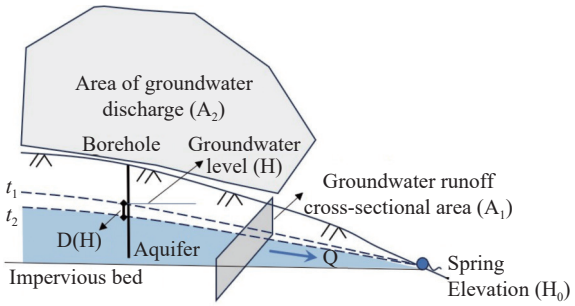

Fig. 4 Diagram of the groundwater discharge in the landslide

A_1, while the surface area of groundwater discharge is approximately A_2. The hydraulic gradient is represented by J. The decline in groundwater level over a unit of time (from t_1 to t_2) is equal to the drainage rate $D(H)$. It is assumed that Darcy's Law can be used to characterize the groundwater discharge. The groundwater discharge Q in a unit of time (from t_1 to time t_2) can be expressed as:

$$Q = KA_1J \tag{2}$$

Where: $J = \frac{H - H_0}{L}$. H_0 is the elevation of spring for the groundwater discharge. L is the distance of groundwater water flow from the borehole to the spring. The groundwater discharge Q can be written as:

$$Q = KA_1\frac{H - H_0}{L} \tag{3}$$

From time t_1 to t_2, groundwater discharge Q can be expressed in another way:

$$Q = D(H)A_2\mu \tag{4}$$

Where: μ is the specific yield of the aquifer. Combining Equations (3) and (4), $D(H)$ can be expressed as:

$$D(H) = \frac{KA_1}{LA_2\mu}H - \frac{KA_1}{LA_2\mu}H_0 \tag{5}$$

The drainage rate $D(H)$ is proportional to the groundwater level in the borehole.

This principle is used by the master recession curve method and demonstrated in Equation (6) (Fig. 3b and 3c).

$$D(H) = a + b \cdot H \tag{6}$$

Where: a and b are fitted parameters using the decreasing groundwater level H and corresponding drainage rate $D(H)$ during the period without rainfall. In Equation (5), $a = \frac{KA_1}{LA_2\mu}H_0$, and $b = -\frac{KA_1}{LA_2\mu}$. The elevation H_0 of springs for the groundwater discharge can be evaluated using the values of $-a/b$. To mitigate the impact of diurnal atmospheric pressure on the groundwater level, the time step for calculating the drainage rate is set at 24 h.

2.4 The cross-correlation function

The Cross-Correlation Function (CCF) represents the relationship between input and output signals. After calculating the cross-correlation between the two signals, the maximum (or minimum if the signals are negatively correlated) of the cross-correlation function indicates the point in time where the signals are best aligned. The time lag corresponding to positive values (larger than the standard error, which will be explained in the later section) of the cross-correlation function is defined as the response time. In this study, the response time obtained from the cross-correlation function between hourly rainfall and corrected hourly increment of groundwater levels corresponds to the mean response time of water level changes in a borehole due to rainfall events. To estimate the time lag with an accuracy of one hour, the corrected hourly increment of the groundwater table induced by the rainfall event was calculated with the following equation:

$$h_t^{Inc} = (h_t - h_{t-1}) + \frac{1}{24}D(h_{t-1})\Delta t \tag{7}$$

Where: h_t^{Inc} is the corrected hourly increment of water table at time t (hour), and h_t is the groundwater table at time t (hour).

The mathematical expression of the cross-correlation function can be written as:

$$C_{rh}(k) = \frac{1}{n}\sum_{t=1}^{n-k}(r_t - \bar{r})\left(h_{t+k}^{Inc} - \overline{h^{Inc}}\right) \tag{8}$$

$$\gamma_{rh}(k) = \frac{C_{rh}(k)}{\sigma_r\sigma_h} \tag{9}$$

Where: C_{rh} is the cross-correlogram, k is the time lag (hours); n is the length (hours) of the time series; r_t is the rainfall in mm at time t (hour); $\bar{r}$ and $\overline{h^{Inc}}$ are the mean values of the rainfall series and hourly groundwater table series respectively; γ_{rh} is the cross-correlation function; σ_r and σ_h are the standard deviation of the time series t and h respectively. To exhibit a significant correlation between the rainfall and the corrected hourly increment time series of the water level, the cross-correlation function must have an absolute value greater than the standard error $2/\sqrt{N}$, where N is the number of data points in the time series. The time range with the cross-correlation value greater than the standard error is the response time of groundwater level to the rainfall.

3 Results and discussions

3.1 Temporal variation in the rainfall, surface displacement, and groundwater table

Fig. 5 presents the daily data of rainfall, surface displacement, and groundwater levels from 1 June 2013 to 12 September 2016. Due to the landslide movement on 7 December 2015, the rain gauge and its cable were destroyed, resulting in missing rainfall data from 8 December 2015 to 1 June 2016. Notably, the groundwater levels in the tension trough (i.e. U1-1) were the highest among all monitoring boreholes, while the groundwater level near the toe front (i.e. U1-5) was the lowest (Fig. 2). The second highest water level was observed at piezometer U1-4, located in the middle part of the landslide.

The groundwater in the landslide is primarily recharged by the precipitation during the rainy period (from June to September). During this time, both the groundwater level and surface displacement increase significantly. For example, in the dry period, the surface displacements of GPS01 and GPS02 were 0.36 mm/d and 0.41 mm/d, respectively. However, in the rainy period, the surface displacements of GPS01 and GPS02 reached 1.61 mm/d and 1.33 mm/d, respectively.

There was a significant positive correlation between the groundwater level in the tension trough (i.e., U1-1) and the surface displacement of the landslide. For example, during a period of heavy rainfall from 15 July, 2013, to 7 August, 2013, the total rainfall amounted to 316 mm. Within this timeframe, the groundwater level at U1-1 increased rapidly by 9.28 m, and the maximum daily surface displacement reached 24.22 mm on 24 July, 2013. Based on the limit-equilibrium theory, Xu et al. (2016) established a relationship between the water level in the tension trough and the slope stability factor, enabling early warning for the Kualiangzi landslide.

By comparing the water level and rainfall time series, it was observed that the groundwater level in the tension trough didn't always exhibit a significant increase during extremely intense precipitation events. For instance, on 9 August, 2014, when the daily rainfall reached 130 mm, the water level in the tension trough increased by less than 1 m. This behavior is noteworthy considering the geological composition of the tension trough, which consists of soil, gravels, weathered rock, breccias, and talus deposit. Notably, the depth of the water level in the tension trough typically exceeded 30 m (Fig. 2).

During a precipitation event, first, the water content of the upper unsaturated zone in the tension trough initially increases to the maximum field capacity. Subsequent rainfall continues to recharge the saturated zone and raises the water table through infiltration. This mechanism results in varying behaviors of groundwater level under different precipitation conditions (such as rainfall intensity, duration, antecedent rainfall). To characterize the water level increment and lag responses to rainfall, the corrected groundwater level incre-

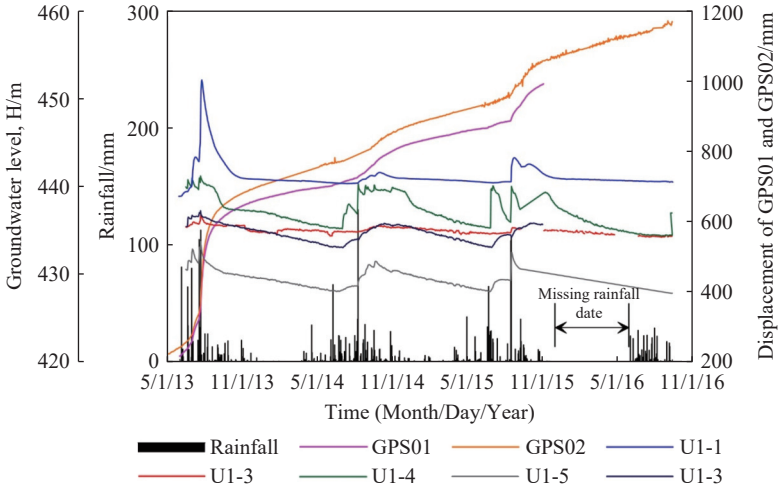

Fig. 5 Daily variations in rainfall, surface displacement, and groundwater level from 1 June 2013 to 12 September 2016. The rainfall recorder and its cable were destroyed by the creeping of landslide on 8 December 2015, which makes the rainfall data from 8 December 2015 to 1 June 2016 missing. The increment in groundwater level (i.e. U1-1) in the tension trough almost kept pace with the displacement rate of the landslide

ments were calculated and several statistical methods were applied in the following sections.

The relationship between the groundwater level in the tension trough (i.e. U1-1) and the displacement rate of GPS01 is presented in Fig. 6. The surface displacement rate is clearly proportional to the groundwater level in the tension trough, indicating that the driving force behind the landslide is the positive pore water pressure (Fan et al. 2009; Xu et al. 2015). Moreover, the curves of the acceleration phase and deceleration phase form a hysteresis loop. Under the same groundwater level conditions, the displacement rate during the deceleration phase exceeds that during the acceleration phase due to the inertia effect. Van Asch proposed a mechanistic model to explain the hysteresis loop in the velocity pattern, considering the role of excess pore pressure in the slow-moving earth flow (van Asch, 2005).

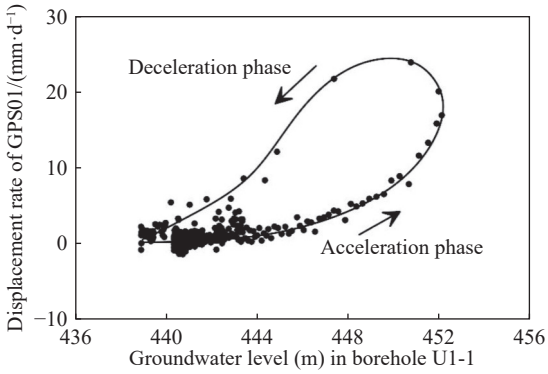

Fig. 6 Relationship between groundwater level in borehole U1-1 and displacement rate of GPS01

3.2 The increment of the groundwater table in boreholes by rainfall

Fig. 7 shows the relationship between the mea-

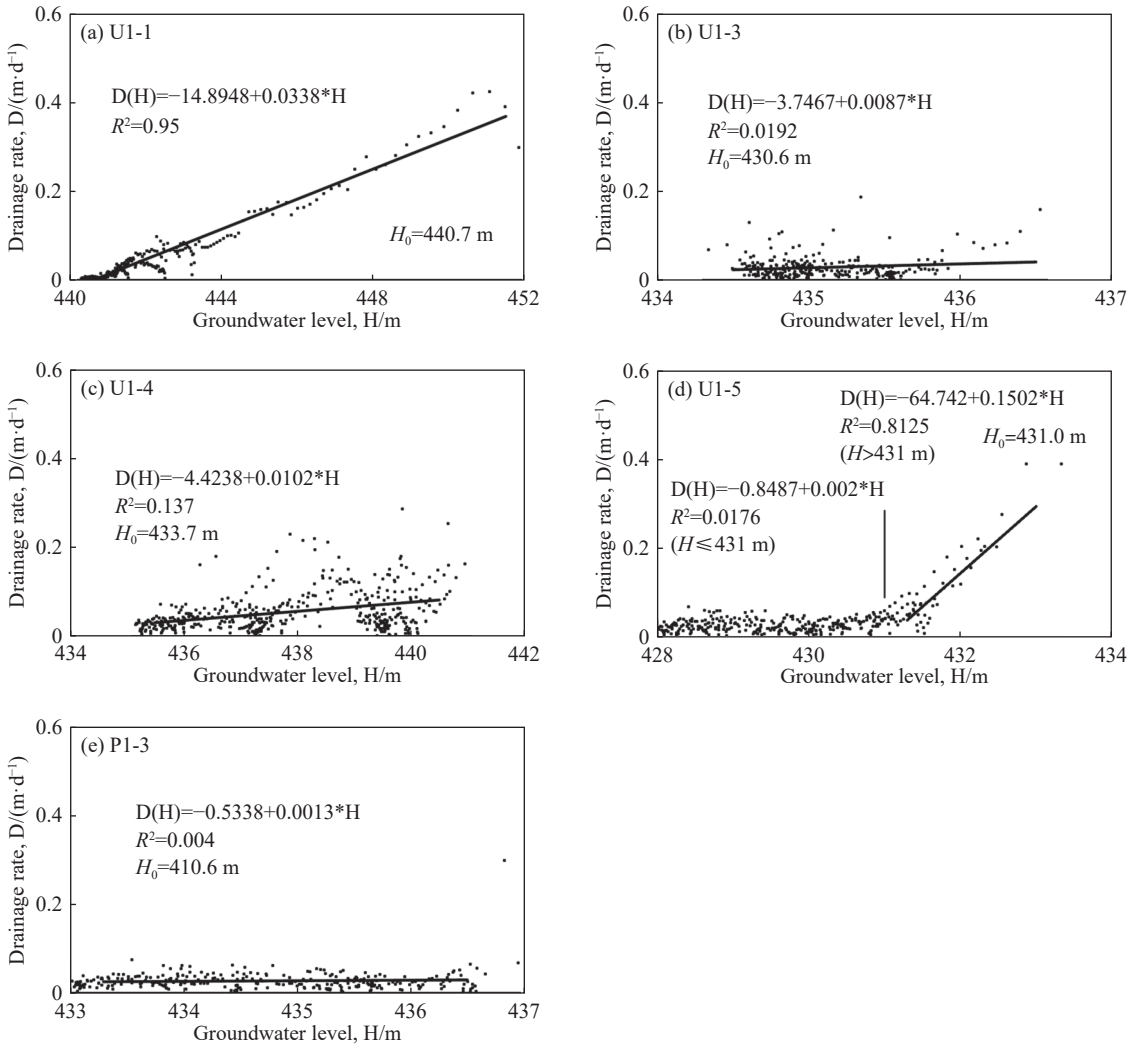

Fig. 7 Relationship between measured water level (H) and drainage rate (D) in boreholes (a) U1-1, (b) U1-3, (c) U1-4, (d) U1-5, and (e) P1-3. The fitted equations relating H and D and their coefficient of determination (R^2) are also given. H_0 is the evaluated elevation of springs for the groundwater discharge

sured water table (H) and drainage rate (D) in boreholes (a) U1-1, (b) U1-3, (c) U1-4, (d) U1-5, and (e) P1-3, using data from the decreasing water table without rainfall. The fitted equations for all boreholes, along with their coefficients of determination (R^2), are provided in the figure. Notably, for borehole U1-1, the drainage rate is directly proportional to the groundwater level. Additionally, the evaluated values of elevation H_0 of springs for groundwater discharge springs range from 410 m to 440 m, which aligns with the actual elevation (390–423 m) of springs on the leading edge (Fig. 1d).

For borehole U1-5, the relationship between drainage rate and water level can be divided into two distinct parts. First, there is a small drainage rate for water table levels less than or equal to 431 m. Second, an apparent relationship emerges for water levels above 431 m. Notably, the elevation of spring on the leading edge aligns closely with the actual elevation 423 m (Fig. 1d). The distance between U1-5 and the spring is approximately 80 m. When the groundwater level at U1-5 exceeds 431 m, the drainage rate significantly increases near the leading edge of landslide.

Based on the relationships between groundwater level and drainage rate in boreholes U1-1 and U1-5, the corrected daily increments of the groundwater table due to the rainfall events from 1 June, 2013, to 31 December, 2015, were calculated according to Eq. 1 and presented in Fig. 8. In the middle part of the landslide (i.e. U1-4, U1-5, and P1-3), the groundwater level responded rapidly to the rainfall, and the increment in water level was typically less than 4 m.

Borehole U1-3 was located in the middle part of the landslide, characterized by relatively steep terrain with an average slope of 0.402. The unsaturated zone had a thickness exceeding ten meters. Due to the steep topography and the substantial unsaturated zone, the majority of precipitation was discharged as surface runoff and lateral interflow. The maximum water table increment observed at U1-3 was only 0.635 m on 22 July, 2013.

Borehole U1-1 was located in the tension trough near the rear edge of landslide. During the dry season and early rainy season, the groundwater level did not exhibit significant increases. However, in the late rainy season, the groundwater level rose noticeably after the water content of unsaturated soil reached its maximum field capacity. Specifically, between 15 July, 2013 and 7 August, 2013, the groundwater level increased by 10.88 m due to a total rainfall of 316 mm. The favorable terrain in the tension trough facilitated rainfall infiltration, and the abundant antecedent rainfall contributed to the increased water content in the unsaturated soil. Consequently, it is assumed that all the rainfall during this period recharged the saturated zone in the tension trough. The specific yield of the unconfined aquifer in the tension trough is 0.029, calculated by dividing the total rainfall of 316 mm by the water level increment of 10.88 m.

Fig. 9 illustrates the monthly variations in cumulative rainfall and water level increment in borehole U1-1, along with Box-Whisker plots showing hourly rainfall for the years 2013, 2014, and 2015. In addition to accumulated rainfall, the intensity of rainfall plays a crucial role in influencing the groundwater table increment in the tension trough. For instance, in July 2013, the total rainfall was 328.5 mm, with a median rainfall intensity of 2.5 mm/d and a third quartiles rainfall intensity of 6 mm/h. During this period, the water level increment in the tension though reached 14.89 m. However, in August 2014, despite a total rainfall of 322.5 mm, the median rainfall intensity was only 1.5 mm/d, and the third quartiles rainfall intensity was 4 mm/h. Consequently, the water level increment in the tension though was merely 1.19 m.

3.3 The lag response of the groundwater table to rainfall

Due to the significant change in the groundwater level (Fig. 8), the hourly groundwater level increment and rainfall data during the rainy period of 2013 were used to analyze the lag response of the groundwater table (Fig. 10). The entire rainy period of 2013 was divided into three distinct events. The first event began on 20 June at 0:00 and end on 29 June at 17:00 with a total rainfall of 91 mm. The second event began on 29 June at 18:00 and end on 15 July at 18:00, with a total rainfall of 120.5 mm. The third event began on 15 July at 19:00 and end on 7 August at 17:00 with a total rainfall of 316 mm.

Fig. 11 illustrates the cross-correlation between rainfall and groundwater level increments at boreholes (a) U1-1, (b) U1-3, (c) U1-4, (d) U1-5, and (e) P1-3 for the three rain events presented in Fig. 9. The lag time of the groundwater table response to rainfall decreases as the cumulative rainfall of the rainy periods increases. This phenomenon occurs because the water content of the unsaturated zone gradually reaches its maximum field capacity, enhancing the unsaturated zone's ability

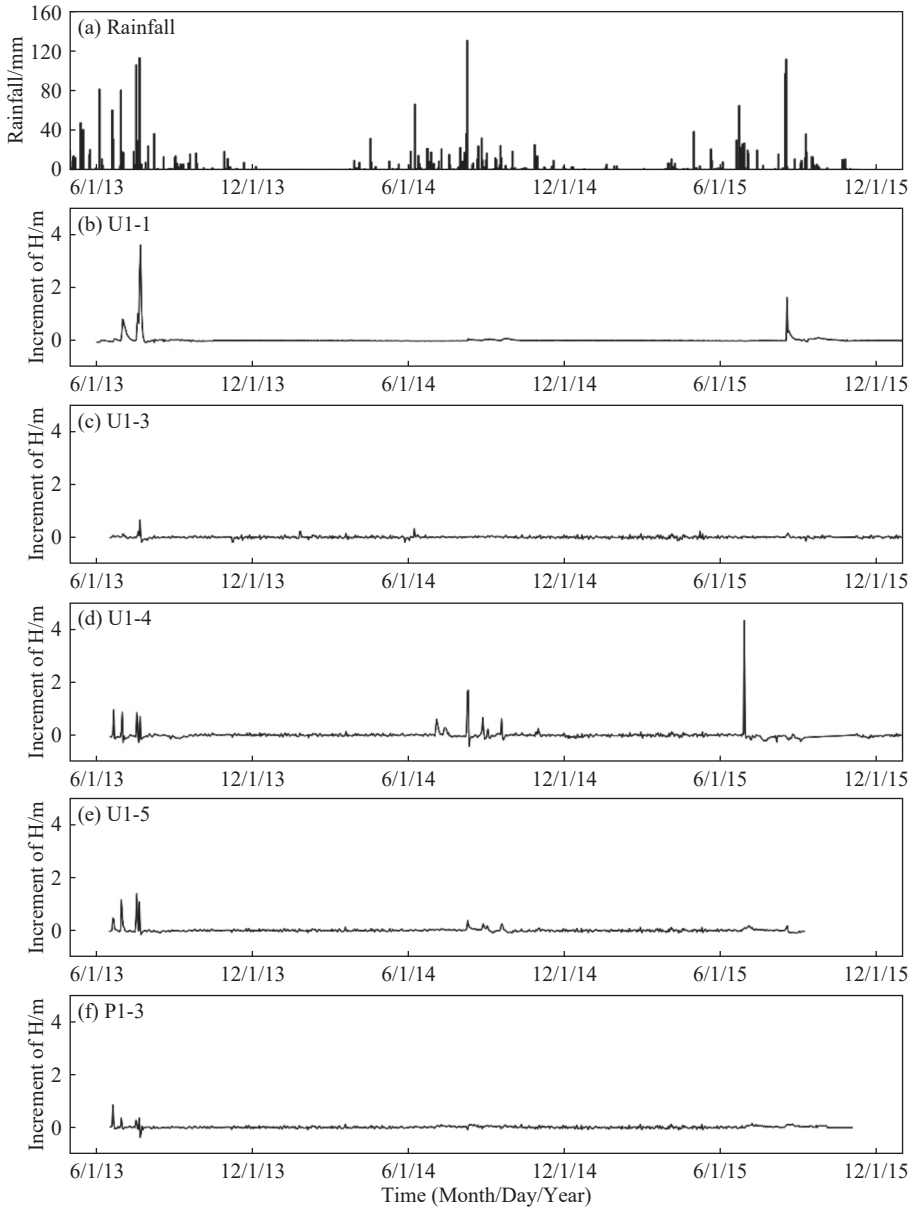

Fig. 8 Daily variations in (a) rainfall and groundwater level increment in boreholes (b) U1-1, (c) U1-3, (d) U1-4, (e) U1-5, and (f) P1-3

to transmit water. Specifically, in borehole U1-1, the minimum lag time for events 1, 2, and 3 were 24 hours, 18 hours, and 0 hours, respectively. The variations in lag time within the tension trough exceeded 24 hours, indicating significant differences in flow rates among different infiltration paths within the complex sediments.

Ling et al. (2016) investigated the internal structure of the southern region of the Kualiangzi landslide using the Electrical Resistivity Tomography (ERT). In their study, the results of A-A' ERT profile near the geological profile I-I' (Fig. 1c and 1d) are shown in Fig. 12. The results revealed interesting features within the landslide area:

(1) There are presences of both a continuous clay layer (less than 15 Ωm) and heterogeneous gravelly soil (greater than 50 Ωm) within the landslide (Fig. 12a). The resistivity image measured in the dry season was taken as a reference model. The resistivity changes during the rainy season, expressed as a resistivity ratio (Fig. 12b), indicate a general decrease in resistivity in the shallow layer. This decrease is attributed to an increase in water content within the clay layer due to the frequent rainfall. Importantly, the clay layer and gravelly soil co-exit at the depth of 10–15 m, suggesting the existence of two distinct paths for groundwater recharge.

(2) In the middle part of the landslide, examining the cross-correlation curves at boreholes U1-3, U1-4, U1-5, and P1-3, two distinct peaks can be observed (Fig. 11b-11e). These peaks indicate that

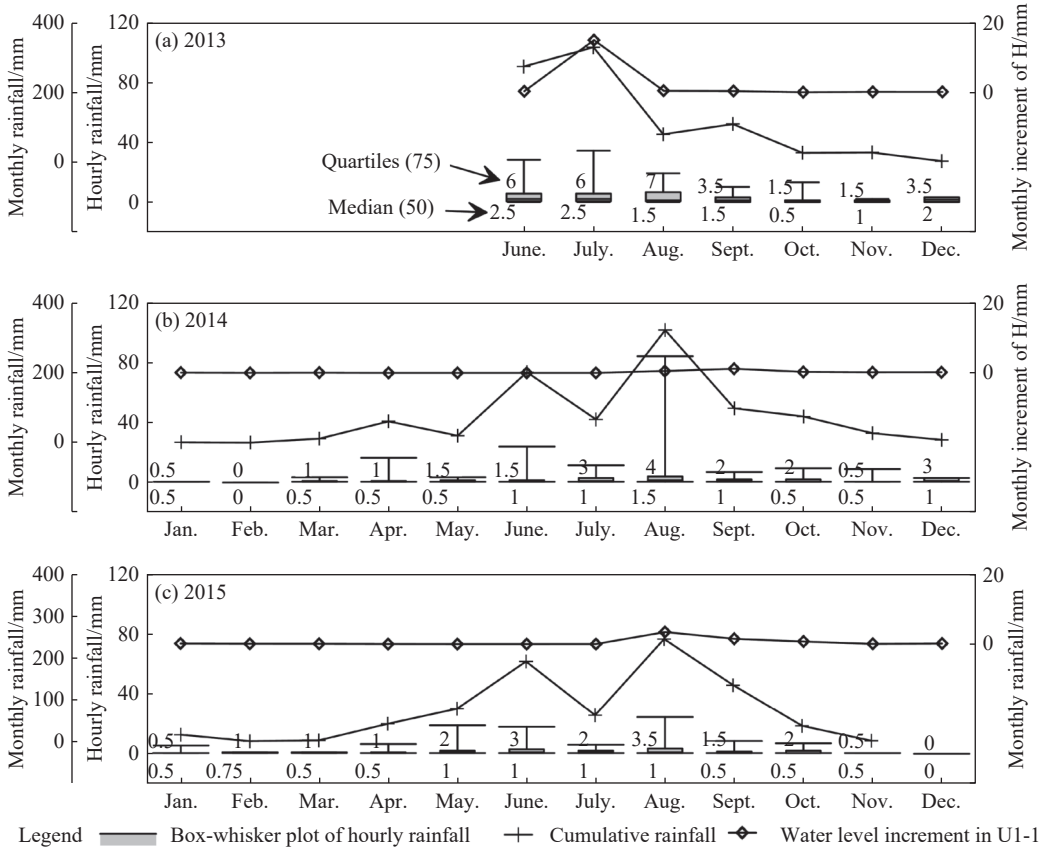

Fig. 9 Monthly variations in cumulative rainfall and water level increment in borehole U1-1, and Box-Whisker plots of hourly rainfall in (a) 2013, (b) 2014, and (c) 2015. The values of median (50) and quartiles (75) were also given in the figures

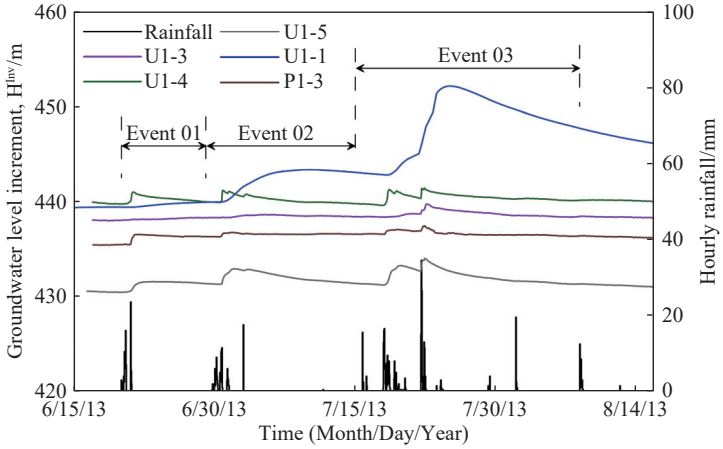

Fig. 10 Hourly variations in rainfall and groundwater level increment from 20 June 2013 to 7 August 2013. The time series of rainfall are divided into three events. The first event was the period from 20 June 0:00 to 29 June 17:00. The second event was the period from 29 June 18:00 to 15 July 18:00. The third event was the period from 15 July 19:00 to 7 August 23:00

there are two responses of the groundwater level to the rainfall. For instance, in borehole U1-5 during event 1, the cross-correlation exhibited peaks at approximately 7 hours and 20 hours. This phenomenon deviates from the typical single-peak cross-correlation curve observed in natural unconfined aquifer (Cai and Ofterdinger, 2016).

The presence of two peaks in the cross-correlation curves suggests that rainfall-induced water movement within the vadose zone of the landslide occurs through two distinct pathways. The first pathway likely involves vertical cracks or frac-

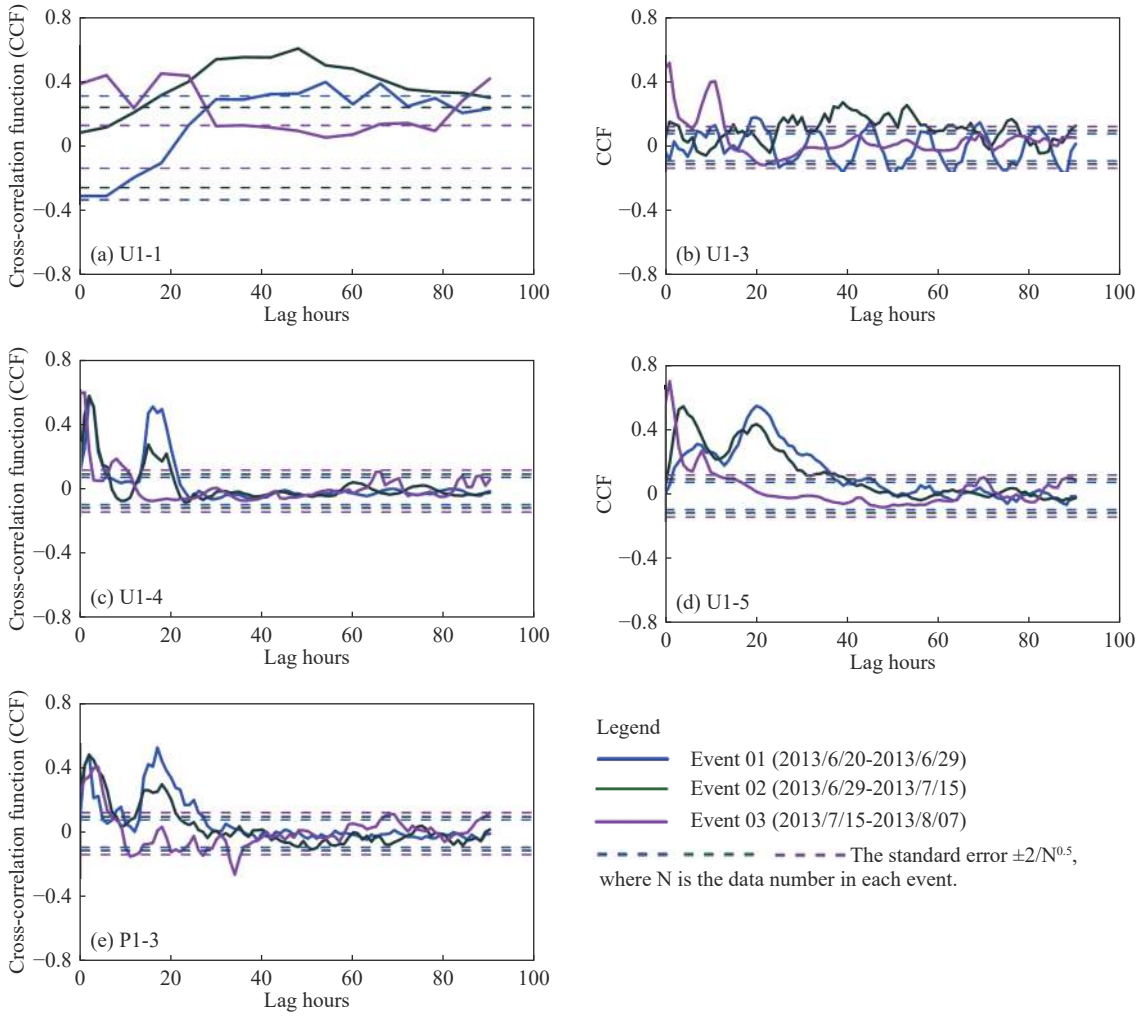

Fig. 11 Cross-correlation between rainfall and groundwater level increment for boreholes (a) U1-1, (b) U1-3, (c) U1-4, (d) U1-5, and (e) P1-3

tures resulting from the slow movement of the landslide. Hydrological tests conducted by Lv et al. (2019) revealed that the hydraulic conductivity along these cracks can be remarkably high, reaching 813.6 m/d. Consequently, water can rapidly propagate to greater depth through these preferential flow paths, leading to the first peak observed in Fig. 11. The second pathway involves the matrix pore space within the unconsolidated sediment, where the flow rate is relatively slow, corresponding to the second peak in Fig. 11.

With frequent rainfall, both the water content of the unsaturated soil and the flow rate within the vadose zone increase significantly. As a result, the lag times between rainfall events and groundwater level responses decrease noticeably for the three events studied. For instance, in borehole U1-5 during event 3, the two peaks occurred at approximately 1 hour and 8 hours after the onset of rainfall. In addition, the behavior of the peaks varies with increasing precipitation. The first peak values of the cross-correlation tend to increase with higher rainfall amounts. This suggests that uniform flow (through the matrix pore space) plays a more important role during the early rainy period. Conversely, the second peak values decrease with increasing precipitation, indicating that preferential flow (via cracks and fractures) becomes more significant during the later rainy period.

4 Conclusion

The groundwater level decreases from the tension trough to the leading front of the landslide in during the rainy season. There exists a significant positive correlation between the groundwater level within the tension trough and the surface displacement of the landslide. As for the lag time of the groundwater table response to rainfall, it decreases with the cumulative rainfall during the rainy periods.

In the middle part of the landslide, two distinct

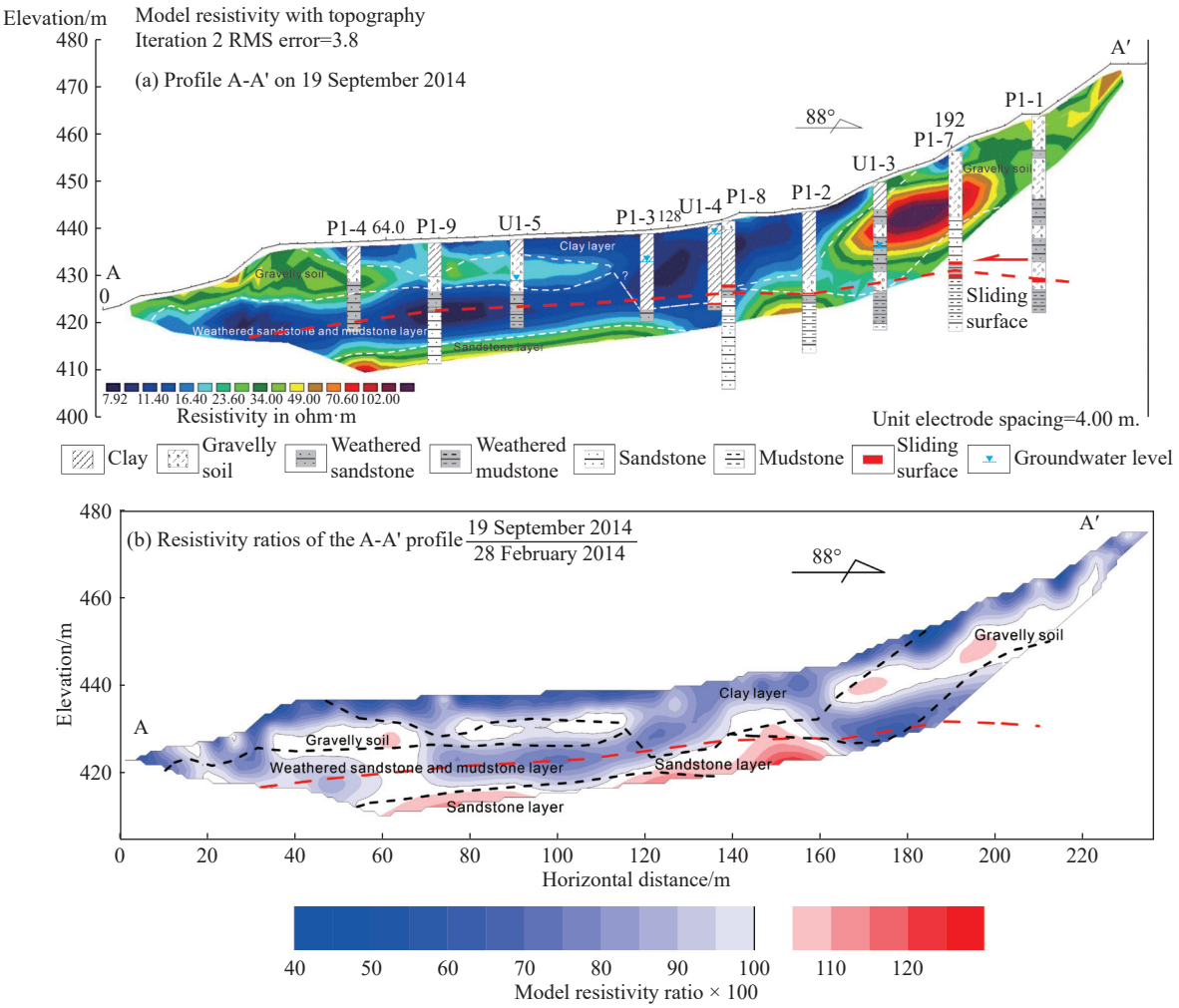

Fig. 12 Electrical resistivity tomography results: (a) the profile A-A' on 19 September 2014; (b) resistivity ratios of the A-A' profile on 19 September 2014, considering the data set of 28 February 2014 as a reference (Modified from Ling et al. 2016)

responses are observed between rainfall and groundwater level These responses manifest as two peaks in the cross-correlation curves, implying that the movement of water from rainfall occurs through two pathways within the vadose zone of the landslide. The first pathway likely involves the vertical cracks or fractures resulting from the slow movement of landslide, allowing rapid water propagation. The second pathway corresponds to the matrix pore space within the unconsolidated sediment, where flow rates are relatively slower. During the early rainy period, uniform flow (through the matrix pore space) dominates, while preferential flow (via fractures) becomes more significant in the later rainy period.

Acknowledgements

This research is part of the "Survey and warning zonation of huge geological hazards in Southwestern China" project (No. 12120113010100), which is supported by the China Geological Survey, and the "Application of electrical resistivity tomography to evaluate the temporal and spatial variation in matric suction of landslide" project (No. 41402268), which is supported by the National Natural Science Foundation of China. This work was supported by the State Key Laboratory of Geohazard Prevention and Geoenvironment Protection (Chengdu University of Technology) (No. 2007DA810083). We are grateful to Theo van Asch for his careful readings and suggestions. We thank the editor and referee for the useful comments.

References

Bernardie S, Desramaut N, Malet JP, et al. 2015. Prediction of changes in landslide rates induced by rainfall. Landslides, 12(3):

481−494. DOI：10.1007/s10346-014-0495-8.

Cai ZS, Ofterdinger U. 2016. Analysis of groundwater-level response to rainfall and estimation of annual recharge in fractured hard rock aquifers, NW Ireland. Journal of Hydrology, 535: 71−84. DOI：10.1016/j.jhydrol.2016.01.066.

Ciupak M, Ozga-Zielinski B, Adamowski J, et al. 2015. The application of Dynamic Linear Bayesian Models in hydrological forecasting: Varying Coefficient Regression and Discount Weighted Regression. Journal of Hydrology, 530: 762−784. DOI：10.1016/j.jhydrol.2015.10.023.

Crosbie RS, Doble RC, Turnadge C, et al. 2019. Constraining the magnitude and uncertainty of specific yield for use in the water table fluctuation method of estimating recharge. Water Resources Research, 55(8): 7343−7361. DOI：10.1029/2019wr025285.

Fan XM, Xu Q, Zhang ZY, et al. 2009. The genetic mechanism of a translational landslide. Bulletin of Engineering Geology and the Environment, 68(2): 231−244. DOI：10.1007/s10064-009-0194-1.

Glade T, Crozier MJ. 2005. The nature of landslide hazard impact. In: Glade T, Anderson M, Crozier MJ. (eds) Landslide hazard and risk. Wiley, New York: Academic Press: 43–74.

Healy RW, Cook PG. 2002. Using groundwater levels to estimate recharge. Hydrogeology Journal, 10(1): 91−109. DOI：10.1007/s10040-001-0178-0.

Hong YM, Wan S. 2011. Forecasting groundwater level fluctuations for rainfall-induced landslide. Natural Hazards, 57(2): 167−184. DOI：10.1007/s11069-010-9603-9.

Hou RN, Chen NS, Hu GS, et al. 2022. Characteristics, mechanisms, and post-disaster lessons of the delayed semi-diagenetic landslide in Hanyuan, Sichuan, China. Landslides, 19(2): 437−449. DOI：10.1007/s10346-021-01751-0.

Jan CD, Chen TH, Lo WC. 2007. Effect of rainfall intensity and distribution on groundwater level fluctuations. Journal of Hydrology, 332(3−4): 348−360. DOI：10.1016/j.jhydrol.2006.07.010.

Labrecque G, Chesnaux R, Boucher MA. 2020. Water-table fluctuation method for assessing aquifer recharge: Application to Canadian aquifers and comparison with other methods. Hydrogeology Journal, 28(2): 521−533. DOI：10.1007/s10040-019-02073-1.

Leng YY, Kong XZ, He JY, et al. 2022. The July 10, 2020, red-bed landslide triggered by continuous rainfall in Qianxi, Guizhou, China. Landslides, 19(6): 1421−1433. DOI：10.1007/s10346-022-01851-5.

Ling CP, Xu Q, Zhang Q, et al. 2016. Application of electrical resistivity tomography for investigating the internal structure of a translational landslide and characterizing its groundwater circulation (Kualiangzi landslide, Southwest China). Journal of Applied Geophysics, 131: 154−162. DOI：10.1016/j.jappgeo.2016.06.003.

Luna LV, Korup O. 2022. Seasonal landslide activity lags annual precipitation pattern in the Pacific northwest. Geophysical Research Letters, 49(18): e2022GL098506. DOI：10.1029/2022gl098506.

Lv HB, Ling CP, Hu BX, et al. 2019. Characterizing groundwater flow in a translational rock landslide of southwestern China. Bulletin of Engineering Geology and the Environment, 78(3): 1989−2007. DOI：10.1007/s10064-017-1212-3.

Maréchal JC, Perrochet P, Caballero Y. 2023. Computing natural recharge using the water-table fluctuation method: Where to site an observation well. Hydrogeology Journal, 31(7): 1991−1995. DOI：10.1007/s10040-023-02707-5.

Nimmo JR, Horowitz C, Mitchell L. 2015. Discrete-storm water-table fluctuation method to estimate episodic recharge. Ground Water, 53(2): 282−292. DOI：10.1111/gwat.12177.

Sahoo S, Jha MK. 2013. Groundwater-level prediction using multiple linear regression and artificial neural network techniques: A comparative assessment. Hydrogeology Journal, 21(8): 1865−1887. DOI：10.1007/s10040-013-1029-5.

Shah B, Alam A, Bhat MS, et al. 2023. Extreme precipitation events and landslide activity in the Kashmir Himalaya. Bulletin of Engineering Geology and the Environment, 82(8): 328. DOI：10.1007/s10064-023-03350-w.

Song LF, Yu X, Xu B, et al. 2021. 3D slope reliability analysis based on the intelligent response surface methodology. Bulletin of Engineering Geology and the Environment, 80(2): 735−749. DOI：10.1007/s10064-020-01940-6.

Tesfaldet YT, Puttiwongrak A, Arpornthip T. 2020. Spatial and temporal variation of groundwater recharge in shallow aquifer in the Thepkasattri of Phuket, Thailand. Journal of Groundwater Science and Engineering, 8(1): 10−19. DOI：10.19637/j.cnki.2305-7068.2020.01.002.

Vallet A, Charlier JB, Fabbri O, et al. 2016. Functioning and precipitation-displacement modelling of rainfall-induced deep-seated landslides subject to creep deformation. Landslides, 13(4): 653−670. DOI：10.1007/s10346-015-0592-3.

van Asch TWJ. 2005. Modelling the hysteresis in the velocity pattern of slow-moving earth flows: The role of excess pore pressure. Earth Surface Processes and Landforms, 30(4): 403−411. DOI：10.1002/esp.1147.

Wen BP, Wang SJ, Wang EZ, et al. 2004. Characteristics of rapid giant landslides in China. Landslides, 1(4): 247−261. DOI：10.1007/s10346-004-0022-4.

Xu Q, Liu HX, Ran JX, et al. 2016. Field monitoring of groundwater responses to heavy rainfalls and the early warning of the Kualiangzi landslide in Sichuan Basin, southwestern China. Landslides, 13(6): 1555−1570. DOI：10.1007/s10346-016-0717-3.

Yan Q, Ma C. 2016. Application of integrated ARIMA and RBF network for groundwater level forecasting. Environmental Earth Sciences, 75(5): 396. DOI：10.1007/s12665-015-5198-5.

Yoon H, Hyun Y, Ha K, et al. 2016. A method to improve the stability and accuracy of ANN- and SVM-based time series models for long-term groundwater level predictions. Computers & Geosciences, 90: 144−155. DOI：10.1016/j.cageo.2016.03.002.

Zhai GJ. 2011. Analysis of the basic characteristics and deformation mechanism of Kualiangzi landslide in Zhongjiang. M. S. thesis. Chengdu: Chengdu University of Technology: 16–36.

Zhang M, Yin YP, Huang BL. 2015. Mechanisms of rainfall-induced landslides in gently inclined red beds in the eastern Sichuan Basin, SW China. Landslides, 12(5): 973−983. DOI：10.1007/s10346-015-0611-4.